Title

Cytoplasmic isoleucyl tRNA synthetase as an attractive multistage antimalarial drug target

Journal

Science Translational Medicine, 15(686)

ISSN

1946-6234

Authors

Istvan, Eva S

Guerra, Francisco

Abraham, Matthew

et al.

Publication Date

2023-03-08

DOI

10.1126/scitranslmed.adc9249

Peer reviewed

Published in final edited form as:

Sci Transl Med. 2023 March 08; 15(686): eadc9249. doi:10.1126/scitranslmed.adc9249.

Cytoplasmic Isoleucyl tRNA synthetase as an attractive Multi-stage antimalarial drug target*

Eva S. Istvan[1], **Francisco Guerra**[2], **Matthew Abraham**[2], **Kuo-Sen Huang**[3], **Frances Rocamora**[2], **Haoshuang Zhao**[3], **Lan Xu**[4], **Charisse Pasaje**[5], **Krittikorn Kumpornsin**[6], **Madeline R. Luth**[2], **Haissi Cui**[7], **Tuo Yang**[2], **Sara Palomo Diaz**[8], **Maria G. Gomez-Lorenzo**[8], **Tarrick Qahash**[9,10], **Nimisha Mittal**[2], **Sabine Ottilie**[2], **Jacquin Niles**[5], **Marcus C. S. Lee**[6], **Manuel Llinas**[9,10,11], **Nobutaka Kato**[4], **John Okombo**[12], **David A. Fidock**[12,13], **Paul Schimmel**[7], **Francisco Javier Gamo**[8], **Daniel E. Goldberg**[1,**], **Elizabeth A. Winzeler**[2,**]

[1]Departments of Medicine and Molecular Microbiology, Washington University School of Medicine, St. Louis, MO 63130, USA

[2]Department of Pediatrics, School of Medicine, University of California, San Diego, La Jolla, California 92093, USA

[3]Cepter Biopartners, Nutley, NJ 07110, USA

[4]The Global Health Drug Discovery Institute, Tsinghua University 30 Shuangqing Rd, Haidian District, Beijing, China

[5]Department of Biological Engineering, Massachusetts Institute of Technology, Cambridge, MA 02139, USA

[6]Wellcome Sanger Institute, Wellcome Genome Campus, Hinxton, CB10 1SA, UK

[7]Department of Molecular Medicine, The Scripps Research Institute, La Jolla, CA 92037, USA

[8]Global Health Medicines, GlaxoSmithKline, Severo Ochoa 2, 28760 Tres Cantos, Spain

[9]Department of Biochemistry & Molecular Biology, Pennsylvania State University, University Park, PA 16802, USA

**Corresponding author dgoldberg@wustl.edu (D.E.G.); ewinzeler@health.ucsd.edu (E.A.W.).

Author Contributions

In vitro selections were performed by E.S.I., M.G.G., S.P.D., J.O., and M.A., with input from D.A.F. Drug sensitivity assays on blood and exoerythrocytic stages were performed by S.P.D., M.G.G., E.S.I. and T.Y. Speed of action experiments were designed and carried out by F.J.G. and B.C.F. Whole-genome sequencing was performed by the UCSD Institute for Genomic Medicine Core Facility and analyzed by M.R.L. Allelic replacement experiments were designed and carried out by K.K. and M.C.S.L. Conditional knockdown (cKD) lines were designed and assayed by J.N. and C.F.P. Plasmid constructs for expression of PvcIRS was designed and generated by E.S.I. and expression and purification of the protein was performed by L.X. Design and optimization of the of the luminescence-based biochemical assay was done by D.E.G., N.K., E.S.I., L.X., K.H., and H.Z. S^{35} incorporation experiments were optimized and performed F.R. Metabolomics assays were designed by M.L. and carried out by T.Q. This manuscript was written by E.W., E.S.I., S.O., F.G., F.R., and D.G.

COMPETING INTERESTS

F.-J.G. and M. G. G.-L. are employees of GlaxoSmithKline and F.-J.G. own shares of the company.

[10]Huck Center for Malaria Research, Pennsylvania State University, University Park, PA 16802, USA

[11]Department of Chemistry, Pennsylvania State University, University Park, PA 16802, USA

[12]Department of Microbiology and Immunology, Columbia University Irving Medical Center, New York, New York 10032, USA

[13]Center for Malaria Therapeutics and Antimicrobial Resistance, Division of Infectious Diseases, Department of Medicine, Columbia University Irving Medical Center, New York, New York 10032, USA

Abstract

Development of antimalarial compounds into clinical candidates remains costly and arduous without detailed knowledge of the target. As resistance increases and treatment options at various stages of disease are limited, it is critical to identify multi-stage drug targets that are readily interrogated in biochemical assays. Whole-genome sequencing of 18 parasite clones evolved using thienopyrimidine compounds with submicromolar, rapid-killing, pan-lifecycle antiparasitic activity showed that all had acquired mutations in the *P. falciparum* cytoplasmic isoleucyl tRNA synthetase (cIRS). Engineering two of the mutations into drug-naïve parasites recapitulated the resistance phenotype and parasites with conditional knockdowns of cIRS became hypersensitive to 2 thienopyrimidines. Purified recombinant *P. vivax* cIRS inhibition, cross resistance and biochemical assays indicated a novel, non-competitive, allosteric binding site that is distinct from that of known cIRS inhibitors mupirocin and reveromycin A. Our data show that *Plasmodium* cIRS is an important chemically and genetically validated target for next-generation medicines for malaria.

One Sentence Summary:

Whole genome sequencing of evolved resistant clones and biochemical assays identified and validated *Plasmodium falciparum* cIRS as a promising antimalarial target.

Keywords

tRNA synthetase; malaria; *Plasmodium* ; drug discovery; target

Introduction

Protein translation has been a drug target since the golden age of antibiotic discovery 80 years ago. From early compounds such as tetracyclines and streptomycin (1) to current clinical candidates such as the antimalarial M5717 (2, 3), disruption of microorganism translation has proven fruitful for treating infections. Of particular interest are the aminoacyl tRNA synthetases (aaRSs) that provide building blocks for protein assembly (4). Each of these enzymes activates a specific amino acid by forming an aminoacyl-AMP and then attaches this intermediate to the cognate tRNA with high specificity. There are separate binding pockets for ATP, amino acid, and tRNA. Some aaRSs have an additional editing domain to increase fidelity. Given their critical role in protein synthesis as well as the multiple sites for substrate recognition and binding, aminoacyl tRNA synthetases provide

a good starting point for developing antimicrobials (5). Inhibitors that target each of the pockets have been described. Three aaRS-targeting drugs are in clinical use: mupirocin (antibacterial), tavaborole (antifungal) and halofuginone (anticoccidial). The first two are topical formulations and the third is veterinary, with each limited by bioavailability and/or toxicity concerns.

The aaRS enzymes of *Plasmodium*, the causative agent of malaria, have recently been of intense interest. This protozoan parasite has 36 aaRSs, Some are cytoplasmic, others organellar (residing in the mitochondrion or apicoplast), and a few are dual-targeted to both the cytoplasm and apicoplast (e.g. PfARS (PF3D7_1367700)) (6). Inhibitors to approximately one dozen of these enzymes have been reported (7). Drug-like, submicromolar compounds that have been identified include cladasporin (cKRS; c for cytoplasmic, K for amino acid lysine), halofuginone (cPRS), benzoxaboroles (cLRS), borrelidin (cTRS), azetidines (cFRS), indolmycin (aWRS; a for apicoplast), and mupirocin (aIRS). Where known, these compounds are slow-killing antimalarials (8), comparable to the translation EF-2 inhibitor M5717 (2) or even second cycle (72-96 h)-acting agents (9, 10).

We report here the identification of *P. falciparum* cIRS as an exciting multi-stage antimalarial target. We further show that its inhibition by thienopyrimidines leads to rapid killing through targeting of a novel, distal binding region that is not subject to competition from the amino acid, nucleoside triphosphate, or tRNA substrates.

Results

Thienopyrimidines have multi-stage activity against P. falciparum

A powerful approach to discovering druggable targets is to begin with compounds active in whole parasite antimalarial screens and to then deconvolute their targets and mechanism of action. MMV1091186 (11), MMV1081413 (from a commercial library that was evaluated for antimalarial activity), MMV019869 (TCMDC124553(12)), and MMV019266 (TCMDC123835 (12)) are four compounds that were identified in various phenotypic screens against asexual or liver-stage parasites and that bear a thienopyrimidine moiety with a thioether bridge (Fig. 1A, Table S2). All have the same core except that the sulfur is located at the C4 position of the pyrimidine ring in MMV1081413. All four have (48 or 72 h) ABS EC_{50} values in the submicromolar range against asexual blood stage parasites (Fig. 1A, Table S2). MMV1091186 has moderate reported liver stage activity but little activity against *P. vivax* hypnozoites (11). Homology searches for molecules with more than 80% identity revealed a variety of closely related compounds with the same core scaffold, including MMV007938 (GNF-Pf-3888), MMV019904 (TCMDC-124602), MMV019837 (TCMDC-124514), MMV062850, MMV020525 (TCMDC-125258), and MMV1328428, all with known blood stage antimalarial activity (Fig. 1). Few showed measurable toxicity against the human cell line, HepG2 (Table S2).

We assessed whether these compounds are likely to be active against multiple lifecycle stages, a high priority qualification for new targets (13). To test activity against sexual stages we used a bioluminescence assay with mature gametocytes (14). MMV1091186

showed submicromolar activity in this assay (Fig. 1B, Table S2). We next tested whether representatives might have chemoprophylactic activity using a liver stage model (15) using two approaches. First, a chemoinformatic substructure search was performed for the core scaffold against a 538,273-compound library that had been tested against *P. berghei* liver stage (11). We observed a primary hit rate of 4% (>75% inhibition for 21,336 compounds), but 146 of the 2051 thienopyrimidines (7%) were active (probability of enrichment by chance 1.37×10^{-11}). In addition, we used empirical testing of select compounds (Fig. 1B). Using a *P. berghei* sporozoite model, HepG2-A16-CD81^{EGFP}(16) cells were pre-incubated with MMV1091186 and MMV19869 24 h prior to sporozoite infection. Bioluminescence measurement was performed at 48 h post-infection to reflect parasite viability. Both compounds demonstrated anti-exoerythrocytic activity at submicromolar concentrations with no cytotoxicity against HepG2-A16-CD81^{EGFP} at 50 μM (Fig. 1C, Table S2). To determine whether the compounds inhibited primarily invasion or liver schizont development, MMV1091186 and MMV019869 were added to plated HepG2-A16-CD81^{eGFP} cells 2 h post-invasion. With this protocol compounds showed higher potency with EC_{50} values a third of those obtained from pre-invasion treatment (Fig. 1C), suggesting a primary effect on liver-stage development. This is in contrast to MMV030084, a cGMP-dependent protein kinase (PKG) inhibitor, that has higher potency (199 nM) against pre-invasion than against post-invasion (>10 μM) (17).

Because targets whose inhibition rapidly leads to parasite death are desirable (13), we next sought to evaluate the parasite reduction ratio (18). To do this, we examined the rate of parasite killing after compound treatment in an asexual blood stage assay. MMV1091186, MMV019869 and MMV019266 all reduced parasitemia *in vitro* very quickly and at a rate that is comparable to that of artesunate, a known fast-acting endoperoxide antimalarial (18) (Fig. 1D). In contrast, pyrimethamine and atovaquone (18) both took over 72 h to eliminate viable parasites at $10\times EC_{50}$.

We also assessed the minimum inoculum of resistance (MIR) for MMV1091186 using a standard method (19). Briefly, selections of *P. falciparum* Dd2-B2 parasites were performed at the 2.5×10^6 to 1.0×10^8 inoculum range. Drug pressure was applied at ~$3.5\times EC_{50}$ (EC_{50} pre-determined in 2-3 independent replicates). Parasite recrudescence was tracked for 30 cycles (60 days) with DSM265 (MIR ~10^6) as a control. After 30 cycles of continuous pressure, we observed no recrudescence for MMV1091186 even in the highest inoculum wells. This corresponds to an estimated MIR value of >10^8. In the DSM265 set-up, parasite recrudescence was observed between days 13 and 27. Parasites appeared in all wells in the 3×10^7 inoculum category and 3/4 wells in the 2.5×10^6 inoculum group, corresponding to an MIR value of ~3×10^6. This value is consistent with the MIR range of 3×10^5 – 1×10^7 routinely observed for DSM265 compound in our experiments (Fig. 1E).

Metabolomics suggest a novel mechanism of action

A previous study had suggested that one of the thienopyrimidines, MMV019837, might target the coenzyme A synthesis pathway (20). To investigate this, we first used metabolomic profiling (21). The parasites were incubated with MMV1091186 or MMV1081413 at $10\times EC_{50}$ for 2.5 h to determine their metabolic response to compound

exposure. A Principal Component Analysis (PCA) scores plot comparing the magnitude of observed effects on a comprehensive set of known metabolites (Fig. S1) suggests a clear differential metabolic profile relative to other established anti-malarial drug classes such as folate biosynthesis inhibitors, mitochondrial (bc1) inhibitors, NCR1 inhibitors, and PfATP4 inhibitors (21). Importantly, we also observed little change in coenzyme A precursors (Table S6). If coenzyme A biosynthesis were indeed inhibited by thienopyrimidines, compound sensitivity should be decreased by inclusion of the product of the pathway (coenzyme A) during parasite dose response experiments. However, we only observed a minimal change in the dose response of wild-type parasites to MMV019869 whether coenzyme A was supplemented or not (Fig. S5A). In contrast, inclusion of 0.8 mM coenzyme A in culture media restored parasite growth and completely rescued the toxicity of panthenol, a characterized inhibitor of the coenzyme A biosynthetic pathway which targets pantothenate phosphorylation (Fig. S5B).

Parasites evolved against thienopyrimidines acquired mutations in cytoplasmic isoleucyl tRNA synthetase (PF3D7_1332900, PfcIRS)

We next used an *in vitro* evolution and whole genome sequencing approach that has yielded the targets of a variety of antimalarial compounds (22, 23). We either employed a gradual ramp-up method that results in more genome replication events and parasites than the standard MIR assay that had failed to generate resistant parasites or started with higher numbers of parasites. Drug resistance in *P. falciparum* was evolved *in vitro* against three thienopyrimidine compounds. Selections for two compounds (MMV1081413, MMV019869) were performed on the Dd2 strain of *P. falciparum*, while the 3D7 strain was used as the parent for selections with MMV1091186. For MMV019869, resistance was evolved over a period of 217 days, with each flask subjected to increasing concentrations of compound starting from 2×EC_{50} (to final compound concentration 5x EC_{50}), with daily tracking of culture health by Giemsa-stained blood smears. The resistance selections were stopped after the bulk, polyclonal cultures yielded a 3 to 5× shift in EC_{50} compared to wild-type Dd2. For MMV1081413, resistance was acquired after 6 months of selections during which compound concentrations were slowly increased from 1.5×EC_{50} to 3×EC_{50}. For MMV1091186, 10^9 asexual blood parasites were kept under continuous drug pressure at 3× EC_{50} (1.92 μM) for two weeks at which point the three selected cultures displayed clear resistance when compared to WT 3D7 strain. Analysis of cloned parasites showed approximately a 2-fold, 30-fold, and 2 to 8-fold shift in the EC_{50} values of MMV1081413, MMV1091186, and MMV019869 respectively (Table S2). Parasites also acquired resistance at the gametocyte stage (Fig. S4).

To identify causative mutations, 18 resistant clones and their isogenic parents were whole-genome sequenced to high coverage (~40-120×, Table S4). Variants were identified by mapping the reads of both the resistant clones and their isogenic parents to the 3D7 reference genome and then eliminating mutations that were observed in both. In addition, the genomes were searched for copy number variants with the GATK4 CNV pipeline using panels of normals developed for the 3D7 and Dd2 genetic backgrounds (24). The data showed that the 18 strains contained 42 newly emerged variants in core genes, including 30 nonsynonymous variants (Table S5). No CNVs were observed. Each one of the clones bore

one of seven nonsynonymous variants in PF3D7_1332900, which is predicted to encode *PfcIRS* (Fig. 2A, Table S5). The probability of this happening by chance is 1.2×10^{-12} for both MMV1091186 and MMV1081413 and 1.2×10^{-43} for MMV019869 (Fig. 2B, hypergeometric mean function). No other gene was mutated to this level of significance with $p<1.2\times10^{-12}$ to 1.2×10^{-43}.

Thienopyrimidines target PfcIRS

To confirm that *PfcIRS* genotypes underlie the drug-resistance phenotypes we observed in the *in vitro*-evolved *P. falciparum* clones, we introduced a E180D, V500A and a V500 silent control mutation into a naïve Dd2 background by CRISPR-facilitated allelic replacement (Fig. 2C) and demonstrated that edited lines were significantly more resistant to MMV019869 and MMV1091186 than clones that carried a silent V500 mutation (Fig. 2D). Testing the CRISPR-edited parasite lines against MMV019869 showed little significant difference in sensitivity compared to the corresponding Dd2-evolved lines ($p>0.22$ combined; $p>0.39$ E180D; $p>0.23$ V500A), indicating that the mutations in *PfcIRS* largely drive the phenotype (Fig. 2E, Table S2). This was further supported by similarity in EC_{50}s across clones with the same cIRS mutation, but different secondary mutations (Table S2 and S5).

Conditional knockdown of cIRS sensitizes cells to thienopyrimidines

To further investigate PfcIRS as a putative target for these thienopyrimidines, genetically modified parasites whose cIRS- and aIRS- (aIRS PF3D7_1225100) expression are controlled by an inducible TetR-aptamer system (Fig. 2E), were studied. In this system (25), regulation of the target gene can be controlled at the translational level via the addition or removal of tetracycline analog anhydrotetracycline (aTc) (25); in the presence of aTC (+aTc), target gene production is maintained, while removal of aTc (-aTC) leads to repression of the target gene and as expected, decreased growth demonstrating importance of cIRS for parasite growth (Fig. 2G). We found that the specific downregulation of PfcIRS led to a significant (3 to 4-fold) increase in sensitivity to both MMV019266 and MMV019869, while no difference in sensitivity to either drug was observed upon repression of aIRS expression (Fig. 2H, Table S2). This is consistent with cIRS as the killing target for these thienopyrimidines. We also tested reveromycin A (RM-A), a validated inhibitor of eukaryotic IRSs, as a control and found a significant (3-fold) shift upon repression of cIRS (Fig 2H).

Thienopyrimidines inhibit translation

Given that aaRSs catalyze the first step of protein synthesis, inhibition of these enzymes is likely to result in amino acid deficiency and a subsequent decrease in translation (26-28). To investigate if inhibition of PfcIRS does indeed lead to an attenuation of global translation, we quantified the incorporation of ^{35}S-methionine/cysteine into newly synthesized parasite proteins in the presence of thienopyrimidines, along with a variety of control compounds that have a mechanism of action that is distinct from translation inhibitors (29). A 1 h, $100\times EC_{50}$ treatment with MMV1081413, MMV019869, halofuginone (inhibits PfPRS) (30), and cycloheximide (inhibits general translation), resulted in a profound reduction in ^{35}S incorporation ($p<0.0001$), relative to treatment with the non-translation control

inhibitors atovaquone, chloroquine, epoxomicin, and carmaphycin, demonstrating that these compounds are likely inhibiting protein translation within the parasites (Fig. S2).

cIRS is an assayable enzyme

To develop a biochemical assay as well as to demonstrate on-target activity, we first tried expression of PfcIRS in *E. coli* using the pET expression system with limited success. We then turned to *P. vivax* cIRS which shows ~67% sequence identity with *P. falciparum* cIRS with the same sets of residues aligning in the predicted active sites (Fig. S3). Similar to PfcIRS, PvcIRS could be expressed in *E. coli*, but expression was leaky and the yield minor. We then expressed His_6-tagged PvcIRS in Sf9 insect cells with relatively high yield; 4.6 mg (>85% purity) of PvcIRS was purified from a 4 L culture over His-Trip and gel filtration columns (Fig S6F). Size-exclusion chromatography showed that it is monomeric (Fig. S6D).

Recombinant cIRS is inhibited by thienopyrimidine compounds

cIRS catalyzes the aminoacylation of $tRNA^{ILE}$ in a four-step reaction. The first reaction is the formation of the activated amino acid and consumes ATP. This cIRS-dependent depletion of ATP can be detected using a luminescent Kinase-Glo™ reaction (Fig. 3A, B). The transfer of the activated amino acid to $tRNA^{ILE}$ (reaction step 3) can be measured in a radioactive aminoacylation assay (Fig. 3A). Initial tests with an ATP depletion assay showed luminescence linearity of purified PvcIRS with both enzyme concentration and time (Fig 3B, C).

To measure affinity (and ensure we were using adequate substrate and inhibitor concentrations) we also calculated K_M for enzyme substrates (Fig. 3D, E). PvcIRS has a sub-micromolar K_M for ATP (0.879 μM) and micromolar K_Ms for both ILE (1.457 μM) and tRNA (0.0935 mg/mL or 3.74 μM). Increasing tRNA increased ATP depletion indicating tRNA binding and ATP consumption are coupled. PvcIRS may mischarge $tRNA^{ILE}$ with valine (most commonly, at a rate of roughly 1 error in 71,900 EcIRS enzymatic reaction cycles) and leucine, which is a common feature of IRS enzymes most likely because the aliphatic amino acid tRNA synthetases descended from a common ancestor that indiscriminately charged either isoleucine, leucine, or valine (31, 32). Although cIRS was able to use valine and leucine, the enzyme has a 200-fold preference to catalyze the reaction with isoleucine (K_M =1.47 μM) over valine (K_M =0.313 mM) and 2000-fold preference over leucine (K_M =3.15 mM) (Fig. 3D).

We investigated the potential of thienopyrimidines to inhibit the ATP-consumption assay, and measured inhibition of step 1 (Fig. 3A, E). RM-A was used as a control compound and showed potent inhibition of PvcIRS (IC_{50}=16.0 ± 3.0 nM). Two thienopyrimidine-containing compounds, MMV1091186 and MMV019869 also inhibited the enzyme reactions with IC_{50}s of 0.87 ± 0.25 μM and 2.82 ± 0.37 μM, respectively (Fig. 3F).

Next, to determine whether thienopyrimidines affect transfer of isoleucine to tRNA (step 3) and further validate that thienopyrimidines are specific for Plasmodium cIRS, we measured inhibition of the tRNA aminoacylation reaction using radioactive isoleucine (Fig. 3A, E). With this assay, MMV1091186 was shown to inhibit isoleucine transfer to tRNA with an IC_{50} of 23.8 μM (Fig. 3G).

Modeling indicates resistance-conferring mutations are in an allosteric or editing site

We performed modeling studies to investigate the most likely binding mode for the compounds (Fig. 4A). Isoleucyl tRNA synthetase is a monomeric, class Ia Aminoacyl tRNA synthetase. There are differences between bacterial and eukaryotic class Ia aaRSs in the C-terminal domain, C-terminal zinc finger (Znf), and in binding of mupirocin (bacterial H581 vs eukaryotic N/S; bacterial L/F581 vs eukaryotic I581) (33, 34). We therefore chose the eukaryotic *S. cerevisiae* (64% sequence similarity) cIRS structure (PDB 7d5c; (35)) as a template to construct a homology model of *P. falciparum* cIRS (Fig. 4A). The SccIRS structure is bound by RM-A and an ILE-AMP intermediate located within the catalytic site of the Rossman fold and importantly, no tRNA is bound for this published structure. To help position tRNA within the catalytic domain in our homology model, we used the structure of EcLRS (4AQ7). Features such as the N-terminal catalytic Rossman fold domain, the editing or proofreading connective peptide 1 (CP1) domain inserted within the aminoacylating Rossman fold domain, a C-terminal α-helical anticodon-binding domain, and a tRNA stem loop acceptor (stem-contact fold) domain (31, 36) are all readily identifiable on our model (Fig. 4A). All class I aaRSs contain a HIGH and KMSKS catalytic sequence in the amino acid active site near the α-phosphate of the bound ATP (Fig 4A), including subclass Ia which is composed of IRS, VRS, and LRS (37). In PfcIRS, these sequences are HYGH and KMSKR, respectively, and are near the L810F mutation that is known to increase thiaisoleucine resistance (Fig. 4A).

In our model, the cIRS mutations fall into two sites. The first site is located within the CP1 editing site (S288, W395, V500, C502). The editing site mutations are proximal to the conserved editing catalytic aspartate (D510 based on homology) (38). The second site of mutations (E180, N269) is located at an allosteric site near the Znf/ hinge region that bridges the Rossman fold to the CP1 domain (Fig. 4A). The hinge region is highly conserved in isoleucyl, leucyl, and valyl tRNA synthetases which are all members of IA subclass of synthases (39-41) and is crucial for structural orientation and inter-domain interactions (42, 43). Importantly, the PfcIRS mutations described here are distant from the HYGH and KMSKR sequences.

Thienopyrimidine mutations are not near known, resistance-conferring mutations for other tRNA synthase inhibitors

In many cases resistance-conferring mutations are at or near residues that directly interact with the inhibitor. We compared our mutations to residues that interact with known cIRS inhibitors or that are associated with resistance. Both the editing and allosteric sites are distinct from the predicted binding sites for RM-A in *S. cerevisiae* (15-24 Å from allosteric site or 33-38 Å from the editing site mutations), Ile-AMP intermediate (21-31 Å from the allosteric site or 39-43 Å from the editing site mutations), thiaisoleucine (L810, approximately 33-43 Å from the allosteric site or 47-50 Å from the editing site mutations to L810), or mupirocin (24-32 Å from the allosteric site or 40-44 Å from the editing site mutations – when aligning a bacterial IRS and our model) (Table S8). MRS is related to cIRS and shares a high degree of conservation (31, 44). The allosteric mutations we observe in cIRS (E180 and N269) are distant (22-30 Å) from residues which interact with a pyrazolopyrimidine (in MetRS02) near the hinge connecting the Rossman fold and the CP1

domains in Leishmania major MRS (residues corresponding to Y441, V442, W443; PDB 6SWX) (45).

Thienopyrimidines may bind to an allosteric site

We next performed docking to determine the more likely binding site in our model (Fig. 4A, S7). Using Chemical Computing Group's Molecular Operating Environment (MOE), we ranked all the cavities on the protein surface of the PfcIRS homology model using the PLB (protein binding ligand) index, which considers size, functionality, and extent of solvent exposure. The allosteric site ranked the highest in terms of PLB scores (6.21), followed by the catalytic site (3.58), with the editing site scoring lowest (0.66-0.79). We next determined the best pose by minimization of binding energies for the different thienopyrimidines within the allosteric site which gave binding energies of −6.55 to −7.18 kcal/mol in the allosteric site. Although a lower binding energy could be obtained in the catalytic site (−6.69 to −8.04 kcal/mol), this was not considered as accessible using the PLB index. The pose of all four tested thienopyrimidines in the allosteric site showed a predicted direct interaction with the E180 residue (Fig. S7).

Cross-resistance studies show thienopyrimidines have a different mode of action than thiaisoleucine and reveromycin A

To further establish that thienopyrimidines are binding to a site that is distinct from the binding site for other cIRS inhibitors, we performed cross-resistance tests using inhibitors of other sites (reveromycin) as well as a mutant that is resistant to thiaisoleucine (9, 35). Our two CRISPR-engineered mutants (E180D, V500A), identified from the MMV019869 selection, but not the silent control V500Si were resistant to MMV1091186 (Fig. 4B) but not to RM-A. Likewise, our W395L evolved line (obtained with MMV1081413) was resistant to all tested thienopyrimidines (Fig. 4C). In contrast we found that parasites with the L810F isoleucine binding pocket mutant, which confers resistance to thiaisoleucine, are hypersensitive to all tested thieonopyrimidines compared to wildtype (3D7) (Fig. 4C). These data suggest that there is a functional link between the thienopyrimidine binding pocket and the HYGH catalytic sequence in amino acid binding site within the Rossman fold, even though the resistance conferring mutations are physically distant (Fig. 4A). While thienopyrimidines could bind to the editing, allosteric, or catalytic sites, the allosteric site model is supported by the magnitude of drug resistance, with the mean resistance fold change for the 24 editing domain mutation/EC_{50} compound combinations significantly less ($p < 0.03$) than the mean fold change for the 12 allosteric/EC_{50} combinations (Fig. 4D) and the lack of mutations observed within the catalytic site.

Thienopyrimidines do not compete with ATP, ILE, or tRNA

To further support a novel allosteric mode of binding, we performed detailed kinetic analyses with the recombinant protein to determine whether thienopyrimidines interfere with substrate binding. IC_{50}s were measured at increasing concentrations of either tRNA, ILE, or ATP. Using the ATP depletion assay we established that the IC_{50}s of PvcIRS with MMV1091186 or MMV019869 were unchanged when any of the three substrate concentrations were increased to 15-30 fold molar excess over K_M (Fig. 4E-F).

To address whether thienopyrimidines may interact with residues in the Rossman fold amino acid binding pocket, we measured inhibition of ATP consumption in the presence of either isoleucine or valine (Fig. 4G). MMV019869 and MMV1091186 had similar EC_{50} values with either amino acid substrate, suggesting that the binding pocket of the compounds does not overlap with the Rossman fold amino acid binding site. These data suggest that thienopyrimidines inhibit PvcIRS activity via a non-competitive mechanism.

Discussion

We have shown that a cluster of thienopyrimidines kill malaria parasites by targeting cIRS. The evidence includes mapping of resistance mutations, hypersensitivity of knockdown parasites, inhibition of parasite protein synthesis, inhibition of recombinant enzyme activity and metabolomic analysis. Different from other inhibitors which prevent growth by interfering with protein translation, thienopyrimidines kill parasites rapidly. This suggests that malaria parasites may be especially vulnerable to a block in $tRNA^{ILE}$ charging. Alternatively, *Plasmodium* cIRS may have essential non-translational functions as has been described for vertebrate aaRSs (46).

Some of the bottlenecks in developing tRNA synthetase inhibitors as antimicrobials have been the pathogen acquisition of mutations conferring enzymatic resistance (47-51). Thienopyrimidines are a class of compounds that have a novel, allosteric cIRS inhibition mechanism that may better elude mutational resistance because of the high degree of conservation within the binding region. Indeed, in our studies, resistance evolution occurred only with high numbers of parasites or prolonged inhibitor ramp-up. The compounds target multiple life stages which allows them to be further developed into both chemoprophylatic (via targeting liver stage) and therapeutic agents (via targeting blood stages and gametocytes).

The thienopyrimidine resistance conferring mutations are located either in the editing domain and or in a putative allosteric binding site. We observed that the mutations in the editing site gave a considerably smaller magnitude of resistance compared to the allosteric site mutations (Fig. 4D). Perhaps the editing site mutations are compensatory instead of providing a steric block. Alternatively, it is possible that the distances between the allosteric and editing site are closer than the 30Å predicted by our model. From crystallographic studies on a related Class 1a aaRS, LeuRS from *E. coli*, which also possesses separate catalytic and editing domains, it has been observed that there are coordinated conformational changes in the LeuRS and bound $tRNA^{Leu}$ tertiary structures as the 3’ end of the bound $tRNA^{Leu}$ transfers from the catalytic site to the editing site (39). From prior work comparing the Apo TtIRS vs. tRNA bound SaIRS, the editing domain is seen to rotate and obscure the catalytic domain in the Apo conformation (40). Though the editing domain from EcLRS appears to have been rotated 180° about a vertical axis and reattached to the Rossman fold / catalytic domain, structures from the aminoacylation and the editing domain states demonstrate that not only does the editing site rotate, but that flexible regions in the CP1 Znf motif / hinge region and the junctional domain also undergo dramatic conformational changes during the translocation step (39). It is therefore possible that between the Apo structure and one of the states with tRNA bound, the allosteric site and the editing domain

site are closer together bringing the mutations E180 and N269 closer to the editing domain site mutations.

Within SccIRS, there are 2 additional CP domains, CP2 and CP3, and a core region (aka Zn finger (Znf) motif or Zinc knuckle that is stabilized by hydrogen bonding and lacking a coordinated Zn together with a hinge region composed of 2 anti-parallel β strands) (35, 52, 53). Using SccIRS nomenclature, PfcIRS E180 (EcIRS D96) is located at the distal end of helix α4 from SccIRS (aka α1 in EcMRS) that is one of the helices in the RM-A binding pocket (35). It has been suggested through affinity labeling experiments that α4 (SccIRS) (or α1 EcMRS) is involved in the recognition of the acceptor arm of tRNA (52). In PfcIRS, the Znf motif is formed by hydrogen bonding between S265, C268, S579, S582 that are spaced 3.2-4.1 Å apart in a non-protonated structure. The E180D (and E180Q) mutations are located on the surface of the α4 helix that is directed towards the Znf motif in PfcIRS (Fig. 4A). The N269K mutation is nearby and located near the hinge region. Docking suggests an allosteric site between the α4 helix, the Znf motif, and the hinge region (Fig. S7). From mutational analysis of EcMRS, the Znf motif has been shown to be critical in methionine activation and in transfer of methionine to the tRNA (52).

We hypothesize that the thienopyrimidines interrupt interactions between the conserved Znf motif whose structure is highly conserved within class Ia aaRSs and helix α4 (using SccIRS nomenclature (35)), thus disrupting isoleucine activation (ATP hydrolysis in step 1) and isoleucine transfer to the 3’ end of $tRNA^{ILE}$ (aminoacylation in step 3). Our ATP-based enzymatic assays support this hypothesis as thienopyrimidines non-competitively inhibit ATP hydrolysis. Our radioactive-isoleucine aminoacylation assays also support inhibition of step 3 by showing thienopyrimidines decrease the rate of aminoacylation. From prior IRS experiments demonstrating that efficient ILE-AMP formation is dependent on tRNA binding, it is possible that the thienopyrimidines non-competitively block tRNA translocation or binding, thus preventing CP1 domain reorientation towards the Rossman fold thereby inhibiting catalysis.

In preliminary cell-based assays the thienopyrimidines show very low toxicity against human HepG2 cells. Knowing that thienopyrimidines target IRS, what could account for the difference in potency against *Homo sapiens* and *Plasmodium falciparum* cytosolic IRS? From analyzing multi-sequence alignments, the W395 and V500 editing domain mutations appear to be highly conserved among eukaryotes (*Homo sapiens, P. falciparum, P. vivax, S. cerevisiae*). S288 appears to be conserved between HscIRS, PfcIRS, and PvcIRS with hydrophobic alanine replacing the polar serine in SccIRS. In SccIRS and HscIRS, the non-polar C502 is replaced by polar uncharged amino acids, glutamine (HscIRS) and arginine (SccIRS). Within the allosteric site, N269 is conserved as a polar residue among eukaryotes, remaining asparagine within *Plasmodium spp.* and *H. sapiens*, but replaced by threonine in *S. cerevisiae*. Interestingly, E180 is conserved among *Plasmodium spp.*, but is replaced by aspartic acid in *H. sapiens* and *S. cerevisiae*. E180D confers resistance to thienopyrimidines and could account for the difference in potencies. In humans, eight cytoplasmic tRNA synthetases (cKRS, cLRS, cIRS, cEPRS, cMRS, cQRS, cRRS, cDRS) and 3 aminoacyl-tRNA synthetase-interacting multi-functional proteins (AIMPs 1-3) form the multi-tRNA synthetase complex (MSC) (31, 40, 54). Within this complex, cIRS is

adjacent to cEPRS, cLRS, and cMRS (54). It possible that HscIRS active sites in humans are less accessible when HscIRS helps form the MSC.

Frequently, structural elucidation of evolved or selectively introduced resistance conferring mutations show that the mutations are adjacent (or near) to the binding site of the small molecule inhibitors. Mupirocin, halofuginone, resveratrol, indolmycin, cladosporin, microcin C analogues have been shown to inhibit the catalytic site of aaRS enzymes. A common feature of all the compounds is overlap with either the amino acid, ATP, tRNA, or combination of these substrates' catalytic binding sites (5, 40, 49, 55). In SaIRS, mupirocin resistant mutations are found to lie near the isoleucine or isoleucyl intermediate binding sites (V588F, H67Q, F563L, V631F, G593V) (49). Halofuginone binds to the proline and tRNA binding pockets within PfPRS (and *Toxoplasma gondii* PRS) (56). L482H in PfcPRS induces increased resistance to halofuginone and is adjacent to the proline binding site (30). Cladosporin binds to the ATP binding site of KRS with surrounding mutations I567, G551, and T340 in SccKRS that cause increased resistance to cladosporin (57). Indolmycin, a natural Trp structural analog, competitively inhibits binding of Trp to WRS (40, 58). The H43N mutation in *Bacillus stearothermophilus* WRS causes increased resistance to indolmycin (58). Resveratrol has been shown to bind in the same site as Tyr in HsYRS (59). Microcin C analogues are pro-drugs that are processed within the cell into non-hydrolyzable amino acid – AMP intermediates and have been shown to target DRS, LRS, and ERS (60).

Tavaborole is known to trap the 3' tRNA in the editing site of SccLRS prior to the aminoacylation step (61). Other benzoxaborols (tavaborole analogues) such as AN6426, AN8432, and AN2729 have been shown to target the editing domain of PfLRS. (7, 40, 62, 63). Evolved mutants of *S. cerevisiae* against tavaborole all mapped to the editing domain with T314M, L315V, R316I / R316T, T319I, V400F / V400D, N415D, and S416L surrounding the boron containing adduct (61, 64). The PfcLRS V568L mutation (AN6426) is near the V500A (thienopyrimidines) mutation which is near the terminal tRNA adenine. In the modeled PfcIRS, W395 and V500 / C502 appear to sandwich the adenine of bound tRNA A76. Of note, the tavaborole evolved mutations caused a 32-256 fold resistance change while the thienopyrimidines editing site mutations only caused a 3-5 fold change in resistance. The allosteric site mutations in PfcIRS caused a much larger shift in resistance from 8-50 fold change (Fig. 4D) which by analogy to the magnitude of fold change in resistance for tavaborole in the editing site suggests thienopyrimidines bind in the allosteric site.

Here, we have demonstrated a novel class of small molecule inhibitors that selectively target *Plasmodium spp.* through a likely novel allosteric mechanism against PfcIRS and have low toxicity against human HepG2 cells. Through varied evolutionary pathways, other pathogenic organisms appear to have adopted IRS structures similar to PfcIRS, such as *Mycobacterium tuberculosis*, *Pseudomonas aeruginosa, E. coli, Staphylococcus aureus,* and other *Enterobacteriaceae*. This opens the possibility for developing not only novel and potent antimalarials, but also potentially new antibiotics that could help in the fight against multi-drug resistant organisms, such as MRSA, VRSA, MDR TB, carbapenem-resistant *P. aeruginosa*, and ESBL *E. coli* / *Enterobacteriaceae*. As artemisinin resistance has emerged and spread, developing an arsenal of novel antimalarials is a high priority (13, 65).

Materials and Methods

In vitro cultivation and drug selection of P. falciparum (UCSD/Goldberg)

P. falciparum (Dd2 and 3D7) were used for *in vitro* drug selection. Continuous cultivation was performed under standard conditions as previously described (9, 22, 23).

In vitro cultivation and drug selection of P. falciparum resistant mutants (MMV1091186)

P. falciparum resistant parasites resistant to MMV1091186 were selected using single step drug selections. Briefly, three independent flasks with 10^9 parasites of a clonal line of 3D7 strain were treated with 10 × EC_{50} of MMV1091186 under standard culture conditions. After 2 weeks of treatment all 3 flasks showed parasite growth. Selections for MMV1081413 and MMV019869 were performed against a Dd2 strain using a gradual ramp-up method. Resistance against MMV019869 evolved over 217 days, starting at 2×EC_{50} and ending at 5x EC_{50}. Resistance against MMV1081413 evolved over 6 months, starting at 1.5×EC_{50} and ending at 3×EC_{50}. Bulk cultures were assayed to analyze degree of resistance. Resistant parasites were cloned by limiting dilution.

ABS EC_{50} determination

EC_{50} values of compounds were determined using a standard 48 h ^{3}H-hypoxanthine incorporation assays (66), flow cytometry assays, or fluorescent labeling. Details can be found in supplemental methods.

Liver stage assays

Assays were performed as previously described (11). Briefly, the immortalized HepG2-A16-CD81^{EGFP} line (67) was used for all liver stage assays. *P. berghei* GFP-Luc-SMcon (reference clone 15cy1) (68) sporozoites were freshly obtained by salivary gland dissection of *A. stephensi* mosquitoes (SporoCore, University of Georgia, Athens, GA) and used to infect HepG2-A16-CD81^{EGFP} cells. The thienopyrimidines and positive control (atovaquone) compounds were dissolved in DMSO and serially diluted into a 384-well plate. DMSO was used as a negative control. More details can be found in the supplemental methods.

To investigate if either compound could block sporozoite entry, hepatocytes were pre-incubated with MMV1091186 and MMV19869 24hrs prior to infection with PbGFP-Luc-SMcon. Bioluminescence was subsequently measured using the Promega Luciferase Assay System 48 h post-infection to quantify parasite viability. Alternatively, to investigate the ability of each compound to inhibit growth of exo-erythrocytic stages of *P. berghei* within the hepatocyte, MMV1091186 and MMV19869 were added to HepG2-A16-CD81^{EGFP} 2hrs post-infection, and bioluminescence was measured after 46 h.

Gametocyte assay (14)

P. falciparum gametocytes were cultured, purified, and assayed as previously described (14). Details can be found in the supplemental methods.

Whole genome sequencing analysis

P. falciparum genomic DNA (gDNA) samples were sequenced and analyzed as previously described (22, 69), with reads aligned to the 3D7 reference genome (PlasmoDB v13.0) via the Platypus pipeline as previously described (70). 18 parasite lines (3 wild-type parents and 15 drug-selected) were sequenced to an average coverage of 70× (Table S3), with an average of 97% of reads mapping to the reference genome (Table S4).

CRISPR/Cas9 gene editing of PF3D7_1332900 (PfcIRS)

Two individual cIRS mutations, E180D and V500A, were successfully validated in isogenic transgenic parasites by CRISPR/Cas9. The synonymous counterpart control for V500 (V500Si) was also constructed. Sequential cloning of the sgRNA and the donor into the plasmid backbone, pDC2-coCas9-gRNA with codon-optimized SpCas9 was performed essentially as described in Adjalley and Lee, 2021 (71). The donor template encoding the mutation of interest and shield mutations at the sgRNA-binding sites was cloned into the AatII/EcoRI sites using NEBuilder HiFi (NEB). Donor and sgRNA insertion were confirmed by Sanger sequencing. Synchronized ring-stage *P. falciparum* Dd2 at 10% parasitemia was collected by centrifugation at 800×g for 5 mins and washed once with cytomix (120 mM KCl, 0.2 mM $CaCl_2$, 2 mM EGTA, 10 mM $MgCl_2$, 25 mM HEPES, 5 mM K_2HPO_4, 5 mM KH_2PO_4; pH 7.6). Packed infected RBCs (150 μL) were mixed with 50 μg plasmid and cytomix to a final volume of 420 μL. The mixture was electroporated using a Bio-Rad Gene Pulser II (0.31 kV, 950 μF), and after recovery for 1 h, spun at 800× g and the pellet washed and cultured in complete media at 3% hematocrit. The next day 5 nM WR92210 (Jacobus Pharmaceuticals) was applied to the culture until day 8, at which point drug pressure was removed. Parasites that survived WR92210 selection were propagated and clones isolated by using limiting dilution. Acquisition of the mutation of interest was verified by Sanger sequencing. The sgRNA oligos and donor repair templates (Fig. 2C) were synthesized by IDT oligo synthesis and GeneArt (Thermo Fisher Scientific) respectively. Sequences of the sgRNAs and genotyping/sequencing primers are shown in Table S7.

Plasmid construction and parasite transfection for cKD lines

Conditional knockdown (cKD) lines using the TetR-DOZI system of the cytosolic (PF3D7_1332900; PfcIRS) and apicoplast (PF3D7_1225100; PfaIRS) enzymes epitope tagged at their C-terminus with 3xHA were generated using the pSN054 linear vector and transfected into an NF54::pCRISPR line (72, 73). Transgenic lines were maintained in 500 nM anhydrotetracycline (aTc, Sigma-Aldrich 37919) and 2.5 mg/mL of Blasticidin S (RPI Corp B12150-0.1). Parasite growth was monitored by Giemsa smears and Renilla luciferase (RLuc) measurements. Details can be found in the supplemental methods.

Growth assay for cKD lines

Synchronous ring-stage parasites were cultured in triplicate in 96-well U-bottom BD Falcon™ plates in 0 and 50 nM aTc. RLuc levels were measured at 0 and 72 h using the Renilla-Glo(R) Luciferase Assay System (Promega E2750) and the GloMax® Discover Multimode Microplate Reader (Promega). Growth was determined by normalizing RLuc

values, with chloroquine (200 nM)-treated samples serving as a no growth reference. Data were analyzed using GraphPad Prism (version 8; GraphPad Software).

Compound susceptibility assays for cKD lines

Synchronous ring-stage cKD lines were grown in the presence (50 nM for MMV019266 and MMV019869 or 500 nM for RM-A) or absence of aTc with titrated levels of compounds for 72 h. DMSO and chloroquine (200 nM) treatment, respectively, served as maximum and minimum growth references for normalization of RLuc levels. EC50 values were obtained from normalized dose-response curves using GraphPad Prism.

P. vivax cyto-IRS protein expression and purification

Full-length cytosolic isoleucyl-tRNA synthetase (PvcIRS, XP_001614116) was codon optimized for insect cell expression. Details on insect cell expression and purification are in the supplement.

PvcIRS ATP consumption luciferase (Kinase-Glo) assay and compound IC_{50} Determination

First, 35 μL of Ile (11.43 μM) or Val (1.14 mM), yeast tRNA (0.40 - 0.46 mg/ml) and ATP (2.5 μM) in Assay Buffer (50 mM HEPES, pH 7.4, 100 mM NaCl, 30 mM KCl, 15 mM $MgCl_2$, 1 mM DTT, 0.04% Tween-20 and 0.2 mg/ml BSA) were added to a 96-well polypropylene plate. After adding 5 μL (200 - 400 nM) PvcIRS per well, the plates were incubated at 37°C for 80 min. Triplicates of 1:1 (10 μL : 10 μL) dilutions of reaction mixture to Kinase-Glo® substrate (Kinase-Glo™ luminescent Kit, Promega) were made on 384-well plates (OptiPlate, PerkinElmer) and incubated at room temperature for 30 min. Luminescence was measured on the VICTOR Multilabel Plate Reader (PerkinElmer).

For IC_{50} determination, test compounds (1 mM stock in DMSO) were diluted (3-fold for MMV019869 and MMV1091186, 2.5-fold for Reveromycin A) in series of 9 concentrations in DMSO and 1.2 μL per well were added into 384-well polypropylene plates (Nunc). 30 μL of 13.73 μM of Ile or 1.373 mM of Val and 0.48mg/ml of yeast tRNA in Assay Buffer (as per above plus 2.5 μM ATP) were added per well, followed by 10 μL of 103 nM PvcIRS, and incubated at 37°C for 80 min. Triplicates of reaction mix to Kinase-Glo® substrate (in 1:1 dilution, 10 μL per ingredient) were added to a 384-well plate and incubated at room temperature for 30 min. 10 μL reaction mix plus 10 μL Kinase-Glo® substrate were added per well to a 384-well plate and incubated at room temperature for 30 min. Luminescence was measured on the VICTOR reader.

For enzyme kinetics experiments, the compound inhibition type is analyzed by a tight binding non-competitive equation in GraphPad Prism:

$$IC_{50} = \frac{[S] + K_M}{\left(K_M/K_i\right) + \left([S]/\alpha K_i\right)} + \frac{[E]}{2}$$

^{3}H-Isoleucine / Valine tRNA Aminoacylation Assay

Purified recombinant PvcIRS was diluted to 0.2 μM and preincubated at RT with varying concentrations of MMV1091186 for 30 minutes (10x of final concentration, < 1% DMSO). 5 mg/mL yeast total tRNA was aminoacylated with radiolabeled isoleucine L-[4,5-^{3}H(N)] (American Radiolabeled Chemicals) by PvcIRS for 15 minutes at 37°C in 50 mM Hepes, pH 7.5, 50 mM KCl, 4 mM ATP, 2 mM DTT, 5 mM $MgCl_2$, 10 μM cold L-isoleucine, 0.004 mg/ml pyrophosphatase. Aminoacylation of tRNA with radiolabeled isoleucine was detected as described by Beebe et al. Counts per second (cps) were measured on a MicroBeta Trilux with Optiphase supermix scintillation cocktail by averaging over 15 seconds (74).

In vitro cultivation of P. falciparum for compound treatments and metabolomic extractions

Metabolite extracts were prepared from purified 3D7 infected RBCs as previously described (21). Details can be found in the supplemental methods.

Metabolomic profiling of drug-treated parasites using mass spectrometry

Extracted samples were prepared as previously described (21), separated using an XSelect HSS T3 2.5 μm C18 Waters column, and run in negative ionization mode on a Thermo Exactive Plus orbitrap (75). Mass spectrometry data was analyzed as previously described (21). All Data is publicly available through the NCBI Metabolomics Workbench (Project ID: PR001318). Details can be found in the supplemental methods.

Minimum Inoculum of Resistance (MIR)

MIR values for MMV1091186 and DSM265 were determined using a modified “Gate Keeper assay” (76). Details can be found in supplemental methods.

Measuring parasite translation using ^{35}S-incorporation

The effect of drug treatment on parasite translation was evaluated by quantifying the incorporation of ^{35}S-labeled amino acids into newly synthesized protein using a protocol adapted from Rottmann *et al* (77). Details can be found in the supplemental methods.

Methods for rate of killing analysis

Rate of killing was assessed using a standardized method (78). Details can be found in the supplemental methods.

Modeling and computational docking

A homology model of PfcIRS (Q8IDZ9; **PF3D7_1332900**) was created using ScIRS (7d5c.1) as a template using Swiss-Model (79). Using Chemical Computing Group's Molecular Operating Environment (MOE), putative binding sites in the PfcIRS homology model were found using geometric algorithms (80-82) and binding energies were calculated for 4 thienopyrimidines. For more details, please refer to the supplemental methods.

Ethical statements

The human biological samples were sourced ethically and their research use was in accord with the terms of the informed consents under an IRB/EC approved protocol

Supplementary Material

Refer to Web version on PubMed Central for supplementary material.

Acknowledgments

We thank Benigno Crespo for support with speed of action studies. We thank Chenguang Zhao at Cepter Biopartners for PvcIRS protein purification.

Funding

EAW is supported by a grant from the NIH (5 R01 AI152533-03). The Bill & Melinda Gates Foundation supported this work with grants to EAW, EI, DG, SO, DAF, MCSL, and ML (OPP1054480) and JN (OPP1132313). MCSL was supported by a grant from Wellcome [206194/Z/17/Z]. M.R.L. was supported in part by a Ruth L. Kirschstein Institutional National Research Award from the National Institute for General Medical Sciences (T32 GM008666). FG was supported in part by a Ruth L. Kirschstein Institutional Research Award (T32 AI007036).

DATA AVAILABILITY

Raw sequencing data for thienopyrimidine-selected parasite samples were deposited in the Sequence Read Archive (www.ncbi.nlm.nih.gov/sra) under BioProject accession PRJNA810479. Raw metabolomics data is publicly available through the NCBI Metabolomics Workbench (Project ID: PR001318). All other data are available in the manuscript and the supplementary materials.

Abbreviations

CP1	connective polypeptide 1
cIRS	cytoplasmic isoleucyl tRNA-synthetase
aIRS	apicoplast isoleucyl tRNA synthetase
aaRS	aminoacyl tRNA synthetase
TPP	target product profile
TCP	target candidate profile
PLB	protein binding ligand
ABS	asexual blood stage

References

1. Krause J, Applications and Restrictions of Integrated Genomic and Metabolomic Screening: An Accelerator for Drug Discovery from Actinomycetes? Molecules (Basel, Switzerland) 26 (2021).
2. Baragana B et al. , A novel multiple-stage antimalarial agent that inhibits protein synthesis. Nature 522, 315–320 (2015). [PubMed: 26085270]
3. McCarthy JS et al. , Safety, pharmacokinetics, and antimalarial activity of the novel plasmodium eukaryotic translation elongation factor 2 inhibitor M5717: a first-in-human, randomised, placebo-controlled, double-blind, single ascending dose study and volunteer infection study. The Lancet. Infectious diseases 21, 1713–1724 (2021). [PubMed: 34715032]
4. Ho JM, Bakkalbasi E, Söll D, Miller CA, Drugging tRNA aminoacylation. RNA biology 15, 667–677 (2018). [PubMed: 29345185]

5. Manickam Y et al. , Drug targeting of one or more aminoacyl-tRNA synthetase in the malaria parasite Plasmodium falciparum. Drug discovery today 23, 1233–1240 (2018). [PubMed: 29408369]
6. Jackson KE et al. , Dual targeting of aminoacyl-tRNA synthetases to the apicoplast and cytosol in Plasmodium falciparum. Int J Parasitol 42, 177–186 (2012). [PubMed: 22222968]
7. Khan S, Recent advances in the biology and drug targeting of malaria parasite aminoacyl-tRNA synthetases. Malar J 15, 203 (2016). [PubMed: 27068331]
8. Baragana B et al. , Lysyl-tRNA synthetase as a drug target in malaria and cryptosporidiosis. Proceedings of the National Academy of Sciences of the United States of America 116, 7015–7020 (2019). [PubMed: 30894487]
9. Istvan ES et al. , Validation of isoleucine utilization targets in Plasmodium falciparum. Proceedings of the National Academy of Sciences of the United States of America 108, 1627–1632 (2011). [PubMed: 21205898]
10. Pasaje CF et al. , Selective inhibition of apicoplast tryptophanyl-tRNA synthetase causes delayed death in Plasmodium falciparum. Scientific reports 6, 27531 (2016). [PubMed: 27277538]
11. Antonova-Koch Y et al. , Open-source discovery of chemical leads for next-generation chemoprotective antimalarials. Science 362 (2018).
12. Gamo FJ et al. , Thousands of chemical starting points for antimalarial lead identification. Nature 465, 305–310 (2010). [PubMed: 20485427]
13. Forte B et al. , Prioritization of Molecular Targets for Antimalarial Drug Discovery. ACS infectious diseases 7, 2764–2776 (2021). [PubMed: 34523908]
14. Lelièvre J et al. , Activity of clinically relevant antimalarial drugs on Plasmodium falciparum mature gametocytes in an ATP bioluminescence "transmission blocking" assay. PloS one 7, e35019 (2012). [PubMed: 22514702]
15. Swann J et al. , High-Throughput Luciferase-Based Assay for the Discovery of Therapeutics That Prevent Malaria. ACS infectious diseases 2, 281–293 (2016). [PubMed: 27275010]
16. Silvie O et al. , Expression of human CD81 differently affects host cell susceptibility to malaria sporozoites depending on the Plasmodium species. Cell Microbiol 8, 1134–1146 (2006). [PubMed: 16819966]
17. Vanaerschot M et al. , Inhibition of Resistance-Refractory P. falciparum Kinase PKG Delivers Prophylactic, Blood Stage, and Transmission-Blocking Antiplasmodial Activity. Cell chemical biology 10.1016/j.chembiol.2020.04.001 (2020).
18. Sanz LM et al. , P. falciparum in vitro killing rates allow to discriminate between different antimalarial mode-of-action. PloS one 7, e30949 (2012). [PubMed: 22383983]
19. Blasco B, Leroy D, Fidock DA, Antimalarial drug resistance: linking Plasmodium falciparum parasite biology to the clinic. Nature medicine 23, 917–928 (2017).
20. Weidner T et al. , Antiplasmodial dihetarylthioethers target the coenzyme A synthesis pathway in Plasmodium falciparum erythrocytic stages. Malar J 16, 192 (2017). [PubMed: 28502250]
21. Allman EL, Painter HJ, Samra J, Carrasquilla M, Llinas M, Metabolomic Profiling of the Malaria Box Reveals Antimalarial Target Pathways. Antimicrobial agents and chemotherapy 10.1128/aac.01224-16 (2016).
22. Cowell AN et al. , Mapping the malaria parasite druggable genome by using in vitro evolution and chemogenomics. Science 359, 191–199 (2018). [PubMed: 29326268]
23. Luth MR, Gupta P, Ottilie S, Winzeler EA, Using in Vitro Evolution and Whole Genome Analysis To Discover Next Generation Targets for Antimalarial Drug Discovery. ACS infectious diseases 10.1021/acsinfecdis.7b00276 (2018).
24. McKenna A et al. , The Genome Analysis Toolkit: a MapReduce framework for analyzing next-generation DNA sequencing data. Genome Res 20, 1297–1303 (2010). [PubMed: 20644199]
25. Goldfless SJ, Wagner JC, Niles JC, Versatile control of Plasmodium falciparum gene expression with an inducible protein-RNA interaction. Nat Commun 5, 5329 (2014). [PubMed: 25370483]
26. Sonenberg N, Hinnebusch AG, Regulation of translation initiation in eukaryotes: mechanisms and biological targets. Cell 136, 731–745 (2009). [PubMed: 19239892]

27. Babbitt SE et al. , Plasmodium falciparum responds to amino acid starvation by entering into a hibernatory state. Proceedings of the National Academy of Sciences of the United States of America 109, E3278–3287 (2012). [PubMed: 23112171]
28. Mazor KM et al. , Effects of single amino acid deficiency on mRNA translation are markedly different for methionine versus leucine. Scientific reports 8, 8076 (2018). [PubMed: 29795412]
29. Obrig TG, Culp WJ, McKeehan WL, Hardesty B, The Mechanism by which Cycloheximide and Related Glutarimide Antibiotics Inhibit Peptide Synthesis on Reticulocyte Ribosomes. Journal of Biological Chemistry 246, 174–181 (1971). [PubMed: 5541758]
30. Herman JD et al. , The cytoplasmic prolyl-tRNA synthetase of the malaria parasite is a dual-stage target of febrifugine and its analogs. Science translational medicine 7, 288ra277 (2015).
31. Bullwinkle TJ, Ibba M, Emergence and evolution. Topics in current chemistry 344, 43–87 (2014). [PubMed: 23478877]
32. Freist W, Sternbach H, Cramer F, Isoleucyl-tRNA synthetase from baker's yeast and from Escherichia coli MRE 600. Discrimination of 20 amino acids in aminoacylation of tRNA(Ile)-C-C-A. European journal of biochemistry 173, 27–34 (1988). [PubMed: 3281834]
33. Nakama T, Nureki O, Yokoyama S, Structural basis for the recognition of isoleucyl-adenylate and an antibiotic, mupirocin, by isoleucyl-tRNA synthetase. The Journal of biological chemistry 276, 47387–47393 (2001). [PubMed: 11584022]
34. Sassanfar M, Kranz JE, Gallant P, Schimmel P, Shiba K, A eubacterial Mycobacterium tuberculosis tRNA synthetase is eukaryote-like and resistant to a eubacterial-specific antisynthetase drug. Biochemistry 35, 9995–10003 (1996). [PubMed: 8756461]
35. Chen B et al. , Inhibitory mechanism of reveromycin A at the tRNA binding site of a class I synthetase. Nat Commun 12, 1616 (2021). [PubMed: 33712620]
36. Nyamai DW, Tastan Bishop O, Aminoacyl tRNA synthetases as malarial drug targets: a comparative bioinformatics study. Malar J 18, 34 (2019). [PubMed: 30728021]
37. Fukai S et al. , Mechanism of molecular interactions for tRNA(Val) recognition by valyl-tRNA synthetase. RNA (New York, N.Y.) 9, 100–111 (2003). [PubMed: 12554880]
38. Fukunaga R, Fukai S, Ishitani R, Nureki O, Yokoyama S, Crystal structures of the CP1 domain from Thermus thermophilus isoleucyl-tRNA synthetase and its complex with L-valine. The Journal of biological chemistry 279, 8396–8402 (2004). [PubMed: 14672940]
39. Bässler H, Köhler A, Charge transport in organic semiconductors. Topics in current chemistry 312, 1–65 (2012). [PubMed: 21972021]
40. Kwon NH, Fox PL, Kim S, Aminoacyl-tRNA synthetases as therapeutic targets. Nature reviews. Drug discovery 18, 629–650 (2019). [PubMed: 31073243]
41. Perona JJ, Hadd A, Structural diversity and protein engineering of the aminoacyl-tRNA synthetases. Biochemistry 51, 8705–8729 (2012). [PubMed: 23075299]
42. Bishop AC, Beebe K, Schimmel PR, Interstice mutations that block site-to-site translocation of a misactivated amino acid bound to a class I tRNA synthetase. Proceedings of the National Academy of Sciences of the United States of America 100, 490–494 (2003). [PubMed: 12515858]
43. Betha AK, Williams AM, Martinis SA, Isolated CP1 domain of Escherichia coli leucyl-tRNA synthetase is dependent on flanking hinge motifs for amino acid editing activity. Biochemistry 46, 6258–6267 (2007). [PubMed: 17474713]
44. Bouz G, Zitko J, Inhibitors of aminoacyl-tRNA synthetases as antimycobacterial compounds: An up-to-date review. Bioorganic chemistry 110, 104806 (2021). [PubMed: 33799176]
45. Torrie LS et al. , Discovery of an Allosteric Binding Site in Kinetoplastid Methionyl-tRNA Synthetase. ACS infectious diseases 6, 1044–1057 (2020). [PubMed: 32275825]
46. Guo M, Schimmel P, Essential nontranslational functions of tRNA synthetases. Nat Chem Biol 9, 145–153 (2013). [PubMed: 23416400]
47. Randall CP, Rasina D, Jirgensons A, O'Neill AJ, Targeting Multiple Aminoacyl-tRNA Synthetases Overcomes the Resistance Liabilities Associated with Antibacterial Inhibitors Acting on a Single Such Enzyme. Antimicrobial agents and chemotherapy 60, 6359–6361 (2016). [PubMed: 27431224]

48. Antonio M, McFerran N, Pallen MJ, Mutations affecting the Rossman fold of isoleucyl-tRNA synthetase are correlated with low-level mupirocin resistance in Staphylococcus aureus. Antimicrobial agents and chemotherapy 46, 438–442 (2002). [PubMed: 11796355]
49. Hurdle JG, O'Neill AJ, Ingham E, Fishwick C, Chopra I, Analysis of mupirocin resistance and fitness in Staphylococcus aureus by molecular genetic and structural modeling techniques. Antimicrobial agents and chemotherapy 48, 4366–4376 (2004). [PubMed: 15504866]
50. Kim SH, Bae S, Song M, Recent Development of Aminoacyl-tRNA Synthetase Inhibitors for Human Diseases: A Future Perspective. Biomolecules 10 (2020).
51. Nass G, Poralla K, Genetics of borrelidin resistant mutants of Saccharomyces cerivisiae and properties of their threonyl-tRNA-synthetase. Molecular & general genetics : MGG 147, 39–43 (1976). [PubMed: 785224]
52. Mechulam Y et al. , Crystal structure of Escherichia coli methionyl-tRNA synthetase highlights species-specific features. Journal of molecular biology 294, 1287–1297 (1999). [PubMed: 10600385]
53. Huang Q et al. , A bridge between the aminoacylation and editing domains of leucyl-tRNA synthetase is crucial for its synthetic activity. RNA (New York, N.Y.) 20, 1440–1450 (2014). [PubMed: 25051973]
54. Khan K, Baleanu-Gogonea C, Willard B, Gogonea V, Fox PL, 3-Dimensional architecture of the human multi-tRNA synthetase complex. Nucleic Acids Res 48, 8740–8754 (2020). [PubMed: 32644155]
55. Rubio Gomez MA, Ibba M, Aminoacyl-tRNA synthetases. RNA (New York, N.Y.) 26, 910–936 (2020). [PubMed: 32303649]
56. Jain V et al. , Structure of Prolyl-tRNA Synthetase-Halofuginone Complex Provides Basis for Development of Drugs against Malaria and Toxoplasmosis. Structure (London, England : 1993) 23, 819–829 (2015). [PubMed: 25817387]
57. Hoepfner D et al. , Selective and specific inhibition of the plasmodium falciparum lysyl-tRNA synthetase by the fungal secondary metabolite cladosporin. Cell Host Microbe 11, 654–663 (2012). [PubMed: 22704625]
58. Hurdle JG, O'Neill AJ, Chopra I, Anti-staphylococcal activity of indolmycin, a potential topical agent for control of staphylococcal infections. The Journal of antimicrobial chemotherapy 54, 549–552 (2004). [PubMed: 15243028]
59. Sajish M, Schimmel P, A human tRNA synthetase is a potent PARP1-activating effector target for resveratrol. Nature 519, 370–373 (2015). [PubMed: 25533949]
60. Van de Vijver P et al. , Synthetic microcin C analogs targeting different aminoacyl-tRNA synthetases. Journal of bacteriology 191, 6273–6280 (2009). [PubMed: 19684138]
61. Rock FL et al. , An antifungal agent inhibits an aminoacyl-tRNA synthetase by trapping tRNA in the editing site. Science 316, 1759–1761 (2007). [PubMed: 17588934]
62. Sonoiki E et al. , Antimalarial Benzoxaboroles Target Plasmodium falciparum Leucyl-tRNA Synthetase. Antimicrobial agents and chemotherapy 60, 4886–4895 (2016). [PubMed: 27270277]
63. Novoa EM et al. , Analogs of natural aminoacyl-tRNA synthetase inhibitors clear malaria in vivo. Proceedings of the National Academy of Sciences of the United States of America 111, E5508–5517 (2014). [PubMed: 25489076]
64. Ottilie S et al. , Adaptive laboratory evolution in S. cerevisiae highlights role of transcription factors in fungal xenobiotic resistance. Commun Biol 5, 128 (2022). [PubMed: 35149760]
65. Talman AM, Clain J, Duval R, Ménard R, Ariey F, Artemisinin Bioactivity and Resistance in Malaria Parasites. Trends in parasitology 35, 953–963 (2019). [PubMed: 31699532]
66. Desjardins RE, Canfield CJ, Haynes JD, Chulay JD, Quantitative assessment of antimalarial activity in vitro by a semiautomated microdilution technique. Antimicrobial agents and chemotherapy 16, 710–718 (1979). [PubMed: 394674]
67. Yalaoui S et al. , Hepatocyte permissiveness to Plasmodium infection is conveyed by a short and structurally conserved region of the CD81 large extracellular domain. PLoS Pathog 4, e1000010 (2008). [PubMed: 18389082]
68. Janse CJ et al. , High efficiency transfection of Plasmodium berghei facilitates novel selection procedures. Mol Biochem Parasitol 145, 60–70 (2006). [PubMed: 16242190]

69. Summers RL et al. , Chemogenomics identifies acetyl-coenzyme A synthetase as a target for malaria treatment and prevention. Cell chemical biology 29, 191–201 e198 (2022). [PubMed: 34348113]
70. Manary MJ et al. , Identification of pathogen genomic variants through an integrated pipeline. BMC Bioinformatics 15, 63 (2014). [PubMed: 24589256]
71. Adjalley S, Lee MC, CRISPR/Cas9 editing of the Plasmodium falciparum genome Methods in Molecular Biology (2021).
72. Nasamu AS et al. , An integrated platform for genome engineering and gene expression perturbation in Plasmodium falciparum. Scientific reports 11, 342 (2021). [PubMed: 33431920]
73. Vanaerschot M et al. , Inhibition of Resistance-Refractory P. falciparum Kinase PKG Delivers Prophylactic, Blood Stage, and Transmission-Blocking Antiplasmodial Activity. Cell chemical biology 27, 806–816 e808 (2020). [PubMed: 32359426]
74. Beebe K, Waas W, Druzina Z, Guo M, Schimmel P, A universal plate format for increased throughput of assays that monitor multiple aminoacyl transfer RNA synthetase activities. Analytical biochemistry 368, 111–121 (2007). [PubMed: 17603003]
75. Lu W et al. , Metabolomic analysis via reversed-phase ion-pairing liquid chromatography coupled to a stand alone orbitrap mass spectrometer. Anal Chem 82, 3212–3221 (2010). [PubMed: 20349993]
76. Duffey M et al. , Assessing risks of Plasmodium falciparum resistance to select next-generation antimalarials. Trends in parasitology 37, 709–721 (2021). [PubMed: 34001441]
77. Rottmann M et al. , Spiroindolones, a potent compound class for the treatment of malaria. Science 329, 1175–1180 (2010). [PubMed: 20813948]
78. Linares M et al. , Identifying rapidly parasiticidal anti-malarial drugs using a simple and reliable in vitro parasite viability fast assay. Malaria journal 14, 1–8 (2015). [PubMed: 25557741]
79. Waterhouse A et al. , SWISS-MODEL: homology modelling of protein structures and complexes. Nucleic Acids Res 46, W296–w303 (2018). [PubMed: 29788355]
80. Edelsbrunner H, Facello M, Ping F, Jie L (1995) Measuring proteins and voids in proteins. in Proceedings of the Twenty-Eighth Annual Hawaii International Conference on System Sciences, pp 256–264 vol.255.
81. Soga S, Shirai H, Kobori M, Hirayama N, Use of amino acid composition to predict ligand-binding sites. J Chem Inf Model 47, 400–406 (2007). [PubMed: 17243757]
82. Volkamer A, Griewel A, Grombacher T, Rarey M, Analyzing the topology of active sites: on the prediction of pockets and subpockets. J Chem Inf Model 50, 2041–2052 (2010). [PubMed: 20945875]
83. Ganesan SM, Falla A, Goldfless SJ, Nasamu AS, Niles JC, Synthetic RNA-protein modules integrated with native translation mechanisms to control gene expression in malaria parasites. Nat Commun 7, 10727 (2016). [PubMed: 26925876]
84. Deitsch K, Driskill C, Wellems T, Transformation of malaria parasites by the spontaneous uptake and expression of DNA from human erythrocytes. Nucleic Acids Res 29, 850–853 (2001). [PubMed: 11160909]
85. Trager W, Jensen JB, Human malaria parasites in continuous culture. Science 193, 673–675. (1976). [PubMed: 781840]
86. Lambros C, Vanderberg JP, Synchronization of Plasmodium falciparum erythrocytic stages in culture. J Parasitol 65, 418–420. (1979). [PubMed: 383936]
87. Kim CC, Wilson EB, DeRisi JL, Improved methods for magnetic purification of malaria parasites and haemozoin. Malar J 9, 17 (2010). [PubMed: 20074366]
88. Agrawal S et al. , El-MAVEN: A Fast, Robust, and User-Friendly Mass Spectrometry Data Processing Engine for Metabolomics. Methods Mol Biol 1978, 301–321 (2019). [PubMed: 31119671]
89. Fang H, Gough J, supraHex: an R/Bioconductor package for tabular omics data analysis using a supra-hexagonal map. Biochemical and biophysical research communications 443, 285–289 (2014). [PubMed: 24309102]

90. Allman EL, Painter HJ, Samra J, Carrasquilla M, Llinas M, Metabolomic Profiling of the Malaria Box Reveals Antimalarial Target Pathways. Antimicrob Agents Chemother 60, 6635–6649 (2016). [PubMed: 27572391]

91. Pang Z et al. , MetaboAnalyst 5.0: narrowing the gap between raw spectra and functional insights. Nucleic Acids Res 49, W388–W396 (2021). [PubMed: 34019663]

92. Gerber PR, Müller K, MAB, a generally applicable molecular force field for structure modelling in medicinal chemistry. Journal of computer-aided molecular design 9, 251–268 (1995). [PubMed: 7561977]

93. Mandt REK et al. , In vitro selection predicts malaria parasite resistance to dihydroorotate dehydrogenase inhibitors in a mouse infection model. Science translational medicine 11 (2019).

94. LaMonte G et al. , Mutations in the Plasmodium falciparum Cyclic Amine Resistance Locus (PfCARL) Confer Multidrug Resistance. mBio 7 (2016).

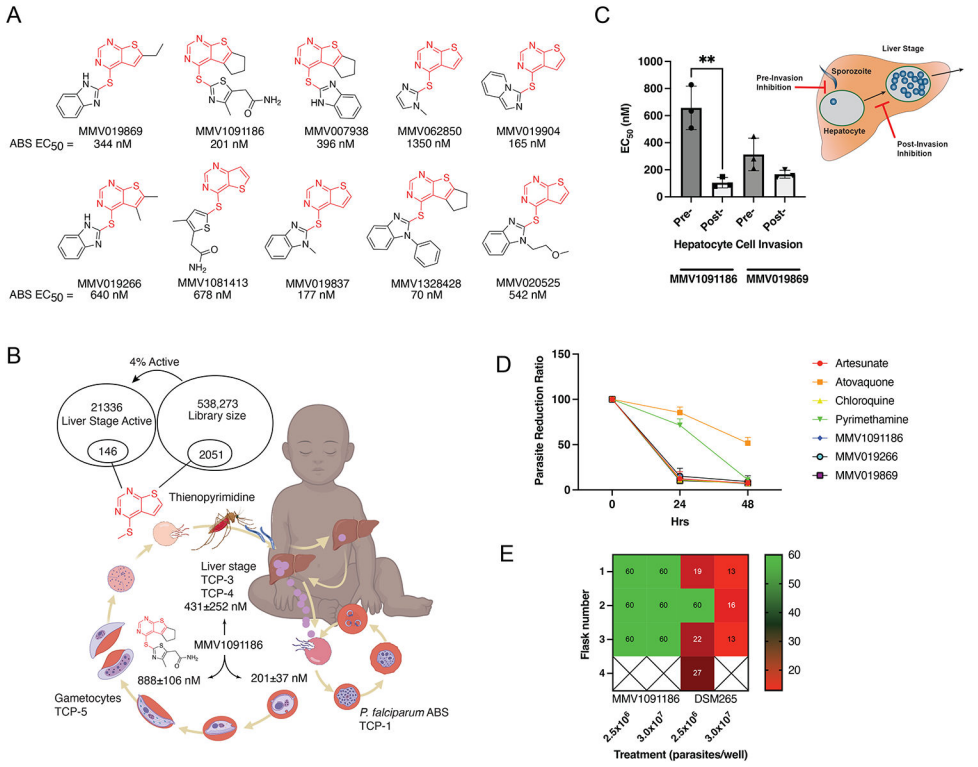

Figure 1.

Thienopyrimidines have multi-life stage inhibition. A) 10 thienopyrimidine compounds (Table S1) with asexual blood stage EC_{50}s. EC_{50}s are reported as the mean against Dd2 background. Technical replicates and statistics are listed in Table S2. B) Malaria life cycle demonstrating these thienopyrimidine compounds have activity at the liver stage, asexual blood stage, and gametocyte stages. Target Candidate Profile (TCP) definitions are described in (13). Initial library of 538,273 compounds has 2051 thienopyrimidines, 146 (4%) of which are active in the Liver stage. MMV1091186 gametocyte activity shown. C) Thienopyrimidine MMV1091186 and MMV019869 pre-invasion vs two hours post-invasion inhibition of *P. berghei* ANKA GFP-Luc-SMcon into HepG2-A16-CD81^{EGFP} cells. Increased potency of MMV1091186 post-invasion is statistically significant at $p<0.004$. Post-invasion EC_{50}s were generally 1/3 of pre-invasion EC_{50}s. D) Parasite reduction ratio measurement demonstrating rate of parasite killing. Data are results of 3 different inocula. E) Minimum inoculum of resistance for MMV1091186 against *P. falciparum* Dd2 background using a parasite inoculum range of 2.5×10^6 to 1.0×10^8 with days to positivity shown; X = none positive up to day 60.

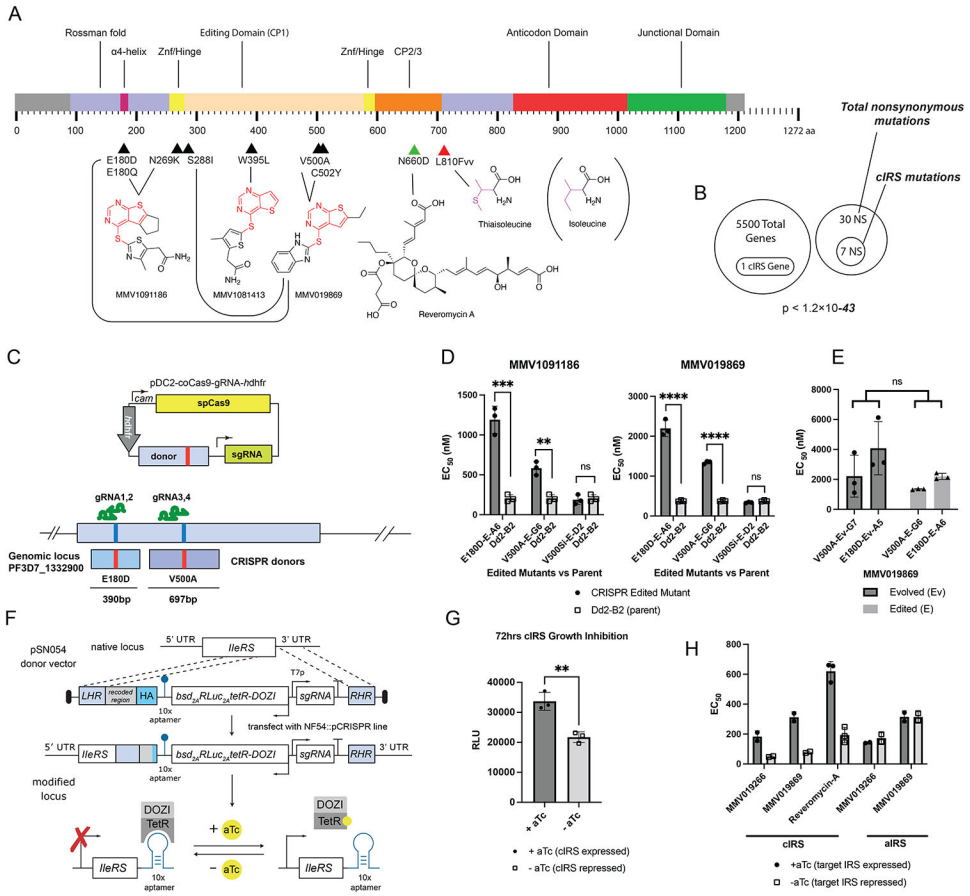

Figure 2.

Genetic validation of cIRS as a target. A) Localization of cIRS mutations withi domains. Tool compound structures shown with lines connecting to associated evolved mutations. B) Significance of identification. Of 5500 total genes in the *P. falciparum* genome, only one cIRS gene is found. The likelihood of identifying 7 nonsynonymous mutations (NS) in 30 total is 1.2×10^{-43} using the hypergeometric mean function. C) System for allelic replacement via CRISPR-Cas9 of E180D, V500A, and V500Si mutants, using two gRNAs per mutant and donor templates with indicated length. D) MMV1091186 and MMV019869 demonstrate increased sensitivity in E180D and V500A mutants, but no change in the V500Si mutant. E) No significant difference between evolved (G7-500A, A5-E180D) and CRISPR edited (G6-V500A, A6-E180D) mutants. F) Diagram of conditional knockdown with cIRS and aIRS expression controlled by an inducible TetR-aptamer system. In the presence of anhydrous tetracycline (aTc), the target IRS is expressed. G) Growth inhibition of conditional knockdowns that show decreased growth with repression of cIRS. 50 μM aTc used in +aTc condition. H) Down-regulation of cIRS leads to a 3-4 fold increase in sensitivity to MMV019266 and MMV019869 and reveromycin-A (RM-A), an established inhibitor of eukaryotic IRSs.

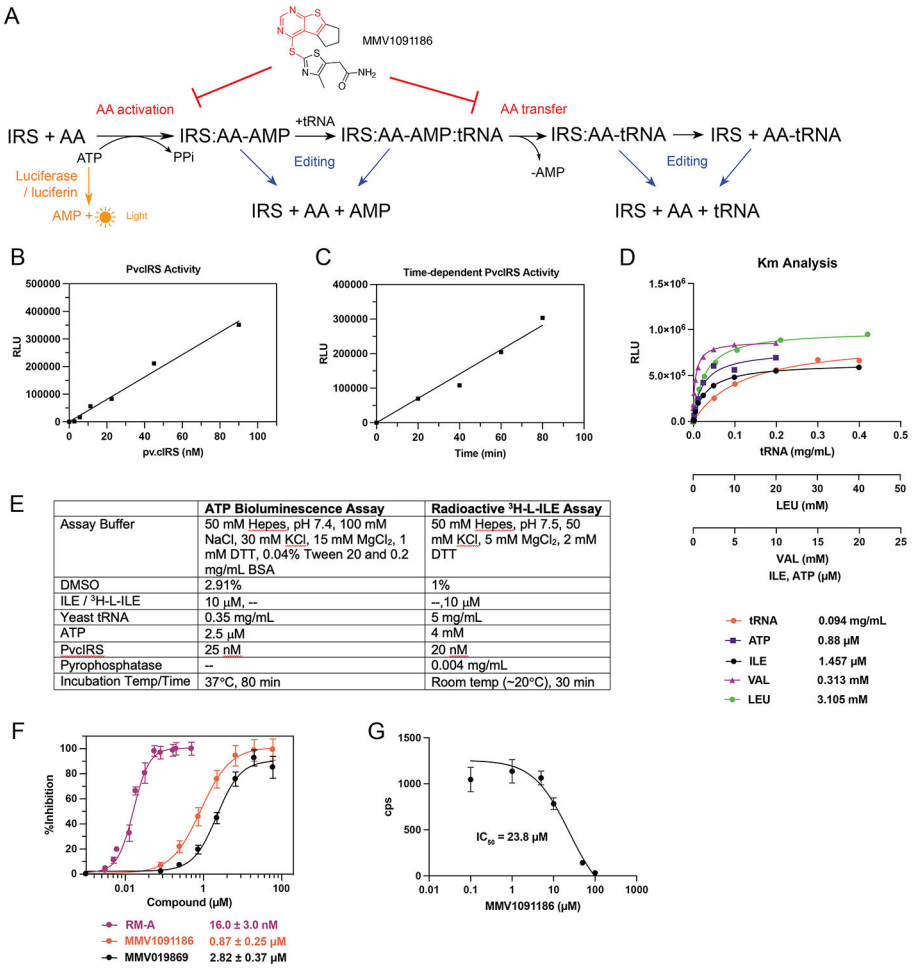

	ATP Bioluminescence Assay	Radioactive ^{3}H-L-ILE Assay
Assay Buffer	50 mM Hepes, pH 7.4, 100 mM NaCl, 30 mM KCl, 15 mM $MgCl_2$, 1 mM DTT, 0.04% Tween 20 and 0.2 mg/mL BSA	50 mM Hepes, pH 7.5, 50 mM KCl, 5 mM $MgCl_2$, 2 mM DTT
DMSO	2.91%	1%
ILE / ^{3}H-L-ILE	10 μM, --	--,10 μM
Yeast tRNA	0.35 mg/mL	5 mg/mL
ATP	2.5 μM	4 mM
PvcIRS	25 nM	20 nM
Pyrophosphatase	--	0.004 mg/mL
Incubation Temp/Time	37°C, 80 min	Room temp (~20°C), 30 min

Figure 3.

Plasmodium cIRS is inhibited by thieonopyrimidines. A) Reaction mechanism of IRS charging of tRNA. ATP based luminescence Kinase-Glo™ assay is detected in the first catalytic step (amino acid activation). Isoleucine charged tRNA is generated in step 3. IRS also removes improperly charged amino acids (leucine, valine) via its editing activity. AA = amino acid. B) PvcIRS activity showing linearity with increasing amounts of enzyme in the Kinase-Glo™ assay. C) PvcIRS activity in Kinase-Glo™ assay (linear over 80 min). D) K_M of different amino acid substrates (Ile, Leu, or Val), ATP, and tRNA in PvcIRS Kinase-Glo™ assay. E) Assay reaction conditions for the ATP bioluminescence-based assay and the ^{3}H-L-ILE tRNA aminoacylation assay. F) Compound concentration-dependent inhibition curves using Ile substrate in the Kinase-Glo™ assay. The average IC_{50} of N=3, n=3 is displayed. G) ^{3}H-ILE aminoacylation IC_{50} curve. MMV1091186 inhibits ILE-tRNA aminoacylation (reaction step 3, the attachment of isoleucine to tRNA) with N=1, n=3.

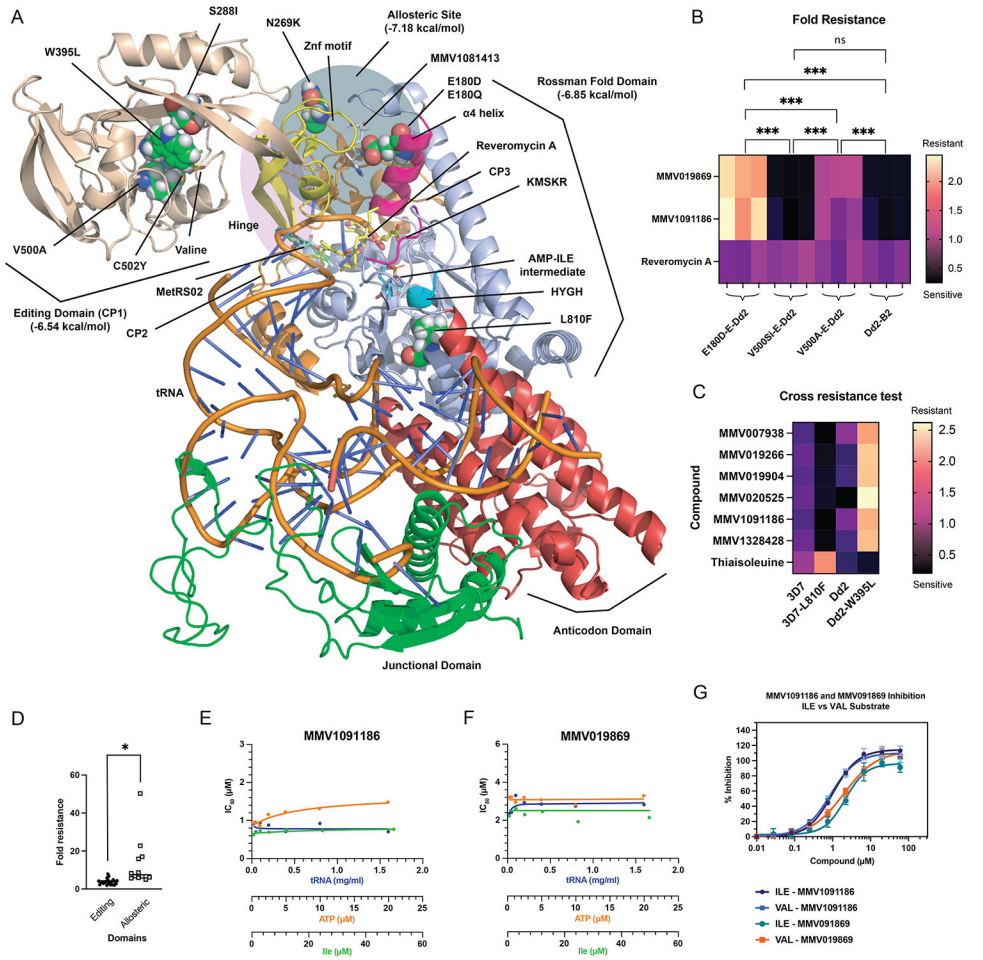

Figure 4.

PfcIRS model and mechanism of inhibition. A) PfcIRS homology model using *S. cerevisiae* structure (7D5C) as a template. tRNA in hairpin conformation based on EcLRS structure (4AQ7). Spheres indicate evolved mutations. Domains are color-coded to match Fig 2A. B) Resistance heat map of CRISPR mutants (V500A, E180D), silent control (V500si) and Dd B2 wildtype EC_{50}s with thienopyrimidines and RM-A. Data were normalized across compounds and are from N=3; n=3 (See Table S2 for raw data). ***p <0.05 using a paired, two tailed t test. C) Cross resistance heat map of EC_{50}s for six additional thienopyrimidine compounds (Fig 1A) and thiaisoleucine (Fig 2A) tested against thienopyrimidine (W395L) and thiaisoleucine evolved mutant (3D7-L810F) for N=1-3; n=3. D) Aggregate fold resistance of editing domain EC_{50}s (S288, W395, V500, C502) vs allosteric domain mutations EC_{50}'s (E180, N269). p<0.03 using Welch's t-test. N (editing domain) = 24; N (allosteric domain) = 12. E, F) IC_{50}s of MMV019869 and MMV1091186 at different substrate concentrations. IC_{50} plotted against tRNA, ATP, and Ile concentrations; alpha close to 1 indicates non-competitive inhibition. G) MMV019869 and MMV1091186 inhibition curves using Ile (10 mM) and Val (1 mM) substrates.